# The effect of lithium wall conditioning in TFTR on plasma–surface interactions

D.N. Ruzic [a,*], Monica M.C. Allain [a], R.V. Budny [b]

[a] *University of Illinois, Urbana IL 61801, USA*
[b] *Princeton Plasma Physics Laboratory, Princeton, NJ 08543, USA*

## Abstract

Five TFTR deuterium supershots with increasing Li pellet injection are analyzed in detail. Five chords of experimental H-α measurements are compared to predictions from a series of computational models. First, experimental data from the discharge is used in the TRANSP plasma transport code to predict the ion flux to the wall. Then a modified version of the DEGAS neutral transport code which includes both reflection, desorption and sputtering of hydrogenic species from the wall is used to determine the neutral density profile across the machine. This data combined with the known density and temperature contours predicts values for the magnitude of H-α light observed for 16 viewing angles of the diagnostic. To match the experimental data, the wall reflection, desorption and sputtering coefficients were altered using data from VFTRIM-3D to include the effect of the added Li. In addition, the first 10 cm of the stainless steel wall adjoining the C inner bumper limiter was treated as C-covered; the highest flux area of the inner wall was treated as a sink; and the lower reflection coefficients for a Li-wall rather than a C-wall were used over an increasingly larger area of the inner wall as the Li concentration in the discharges increased. © 1999 Elsevier Science B.V. All rights reserved.

*Keywords:* Lithium coating; DEGAS Code; Transport modeling; TFTR

## 1. Introduction

The performance of TFTR is greatly enhanced when the carbon inner bumper limiter has been scoured of its imbedded D by the repeated production of high power discharges fueled only by the desorbed gas. When $Z_{eff}$ reaches a value of approximately 6 all of the easily desorbed surface D has been removed. The wall is then fully conditioned and a 'supershot' plasma is formed [1].

In May 1994, a series of supershots were performed keeping all parameters constant except for the addition of Li pellets. The first shot of the series had no Li injection and served as a baseline. The subsequent four shots had the same amount of Li injected into each, thus increasing the total Li content on the walls during the series. The performance of the plasma improved as the total Li content increased. This paper endeavors to explain why in terms of the plasma-surface interactions.

The primary diagnostic used in this work is a spectroscopic measurement of the H-α light emanating from differing chords across the minor radius of the plasma. This data is compared to modeling results for the discharge. In previous work a variety of plasma parameters in the models were altered [2,3] to produce a fit to the data. Changes of that type were inadequate to match the data from these experiments. In this work the only variables changed in the model are the plasma–surface interaction of the ions and neutrals on the walls. These variables include the absorption/re-emission characteristics, the sputtering coefficient of trapped D, and the reflection coefficients.

## 2. Simulation

The TRANSP plasma analysis code is used to model the time evolution of the plasma parameters [3,4]. The

* Corresponding author. Tel.: +1 217 333 0332; fax: +1 217 333 2906; e-mail: druzic@uiuc.edu

energy, particle, and magnetic field dynamics are computed based on the measured plasma profiles and location of the last closed flux surface. The measured inputs include time-dependent profiles of the electron density, electron and carbon temperatures, and carbon toroidal velocity. The plasma scrape-off length used in TRANSP was held constant in all cases at 1.60 cm.

These measured parameters and the ion temperatures and densities taken from TRANSP, as well as the actual geometry of the wall are used as input for DEGAS. DEGAS [5] is a 3D Monte Carlo neutral gas transport code. The neutral atoms are sourced from the ion flux on the wall as specified by the TRANSP output. These neutrals are followed as they undergo ionization, charge exchange, dissociation, and surface interactions. The neutral density profile is produced and the H-α emission along any specified chord can be calculated since the electron density and temperature are known. The light from H-α is summed along sixteen viewing chords five of which overlap the experimental diagnostic measurements (Fig. 1). The total number of ionizations within the core and the total H-α light produced are also determined.

The surface interactions are important to understand the role of Li in these discharges. When a particle strikes the wall it will either reflect or stick based on the energy-dependent reflection coefficients. The particle may also sputter deuterium that is trapped in the surface and/or the wall material. These probabilities and the energy of the reflected or sputtered D atoms are determined by the VFTRIM-3D Monte Carlo code [6] and input as look-up tables in the DEGAS code [7]. Three different surfaces were considered for this work: stainless steel (modeled as iron), deuterium-saturated-carbon (at a

ratio of 4 D to 10 C) and Li. In addition it is possible to circumvent the look-up of VFTRIM-3D reflection coefficients and allow reflection to be zero, or make all the reflection coefficients equal to one. Sputtering can be handled in a similar manner – it can be forced to zero at any particular location.

In DEGAS, particles that do not reflect typically are returned to the simulation as appropriately-weighted wall-temperature molecules. It is possible however to set the absorption coefficient of the wall so that no molecules are returned. This turns out to be one of the most important influences of the wall model on the H-α results. 'No absorption' means that the wall is saturated and for every two ions or atoms that do not reflect, one molecule will desorb. On the other hand if a wall segment does 'absorb' then no molecular flux is returned to the plasma from that point.

## 3. Experiment

The five TFTR discharges examined in this study are # 76649, 76650, 76651, 76653 and 76654 from May 23, 1994. These TFTR supershots were performed after a long series of wall conditioning which desorbed the inner bumper limiter of deuterium. Supershots are circular cross-section plasmas which ride on the inner bumper limiter and are only fueled by the neutral beams. Therefore the interaction with the wall dominates recycling. There was no Li injection in the first shot and then two identical 1.0 mg Li pellets were injected in each of the subsequent four shots at 2.2 and 2.7 s into the discharge 19.7 MW of neutral beam power was added between 3.7 and 4.3 s. The plasma parameters described below and the modeling results all take place at 4.2 s. The major radius was 2.52 m, $I_p = 2.5$ MA and $B_T = 5.1$ Tesla. The standard suite of TFTR diagnostics were available during this series of discharges. In addition five chords of H-α light were recorded from the H-α interference filter array (HAIFA) [8].

The HAIFA views the TFTR inner bumper limiter from the outside midplane. Five absolutely calibrated channels measure H-α emission through views passing through a vertex at a major radius of 396 cm at angles 0, 7.5, 14, 23 and 30 degrees from the midplane. A toroidal variation of light is seen coinciding with the segmentation of the vacuum vessel. The maximum emission is approximately 20% greater than the minimum [9] due to ripple in the toroidal magnetic field. Since the entire HAIFA is pointed at maximum emission points, the measured HAIFA signal is reduced by 10% to give a value indicative of the toroidally averaged emission – the emission which is simulated. Assuming up–down symmetry, as verified by a TV camera filtered to observe near the H-α line, the HAIFA provides a measure of the total emission and the distribution of those emission
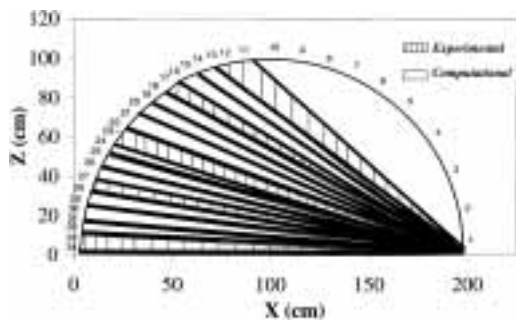


Fig. 1. Upper half of the TFTR minor radius cross-section. The HAIFA diagnostic is to the right of the drawing on the midplane. The wall segments are numbered. The graphite inner bumper limiter extends from segments 14–34. Sixteen chords over which H-α light can be integrated are shown. The five chords that compare to the experimental measurements are shaded. The DEGAS simulation treats the midplane boundary as a mirror – Monte Carlo flights are specularly reflected upon crossing it.

from the bumper limiter, where virtually all of the re-cycling occurs. The absolute error in the magnitude of the emission for each experimental point is about 3% [9], equivalent to the size of the experimental data points in Figs. 2 and 7. The error in the poloidal angle is larger, approximately ± 3 degree.

## 4. Results

The presence of increasing accumulated Li on the walls had several effects. First, the $Z_{eff}$ at 4.2 s increased from 2.3 to 3.0. This increase is inevitable with the ad-dition of an impurity. However, the plasma performance improved dramatically. The total stored energy in-creased from 3 to 4.5 MJ. The central electron line density at that time also increased from 2.5 to $3.9 \times 10^{19}$ $m^{-3}$ due to a peaking of the density profile. The peak electron density (at $r/a = 0$) rose from 5.1 to $6.5 \times 10^{19}$ $m^{-3}$ while the density at $r/a = 0.5$ dropped from 3.0 to $2.3 \times 10^{19}$ $m^{-3}$. The central ion temperature rose from 19 to 43 keV indicating an increase in the energy con-finement time.

These increases in the energy confinement were ac-companied by an increase in particle confinement and a decrease in recycling. The neutral density profile in-creased at the center from 2.6 to $3.9 \times 10^{19}$ $m^{-3}$ but decreased at $r/a = 0.5$ from 1.4 to $0.7 \times 10^{19}$ $m^{-3}$ and at the edge ($r/a = 0.8$) from 1.2 to $0.6 \times 10^{19}$ $m^{-3}$. The wall fueling also dropped from an influx of 2.0 to $1.0 \times 10^{22}$ $s^{-1}$.

The best fit of the predicted H-α chords to the ex-perimentally measured data at 4.2 s for shot 76649 – the baseline case before any Li injection – and shot 76650, the first Li injection shot, are shown in Fig. 2. The mod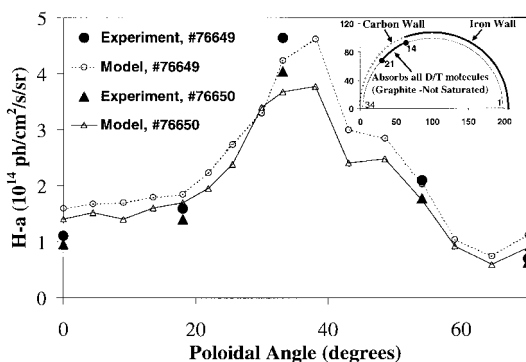eling results from the sixteen chords are overlaid on the five experimental points for each shot. The wall model which led to this fit had the eight segments of the wall which received the highest ion flux (segments 14–21) be totally absorbing. This means that any D ion or neutral that struck the wall and did not bounce off remained buried in the wall. No molecular species were re-emitted. Desorption was allowed from the other segments.

In terms of reflection and sputtering, wall segments 1–13 were treated as iron and wall segments 14–34 were deuterium-filled graphite. (Note that virtually no differ-ence is seen in the calculated atomic reflection and sputtering data between iron and stainless steel.) In the actual device the division between the Fe (stainless steel) wall and the C limiter actually occurs at a higher seg-ment number, but the stainless steel near the limiter is covered with a significant carbon film. Sputtering was allowed to contribute to the plasma – deuterium atoms are sputtered from the carbon surface by the impact of fast deuterium atoms and ions. These sputtered deute-rium atoms have an energy of approximately 8 eV. Ev-idence for the presence of this energy component of D influx has been seen in D-α Doppler broadening mea-surements [7]. Note, even though shot 76650 had Li injection no Li is needed in the wall model to produce the best fit. This is likely due to having less than one monolayer of Li on the critical surfaces after only one injection shot.

Fig. 3 shows the best fit of the predicted H-α chords to the experimental measurements of shots 76651 and 76653. Note that the total emission of H-α light con-tinues to decrease as more Li has accumulated. The wall model which produces this best fit still had no desorp-tion of molecules in segments 14–21, and sputtering of D
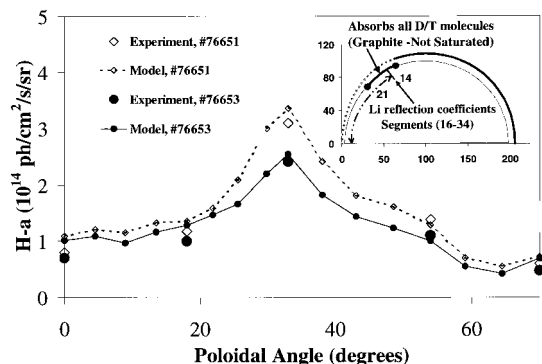


Fig. 2. Experimental and modeling results for TFTR shot #'s 76649 and 76650. The inset shows the wall model used for these two cases. Segments 14–21 absorb all non-reflecting incident particles. Reflection coefficients for D-saturated-C are used for segments 14–34.



Fig. 3. Experimental and modeling results for TFTR shot #'s 76651 and 76653. The inset shows the wall model used for these two cases. Segments 14–21 absorb all non-reflecting incident particles. Reflection coefficients for D-saturated-C are used for segments 14 and 15, while reflection coefficients for Li are used for segments 16–34.
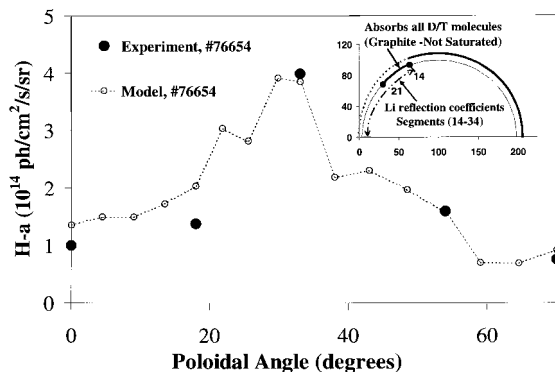
Fig. 4. Experimental and modeling results for TFTR shot # 76654. The inset shows the wall model used for this case. Segments 14–21 absorb all non-reflecting incident particles. Reflection coefficients for Li are used for segments 14–34.



Fig. 5. The effects of altering which segments absorb non-reflecting incident particles is shown for shot 76653.

from segments 14–34, but used the reflection coefficients for Li instead of C for segments 16–34.

Fig. 4 shows the best fit of the predicted H-α chords to the experimental measurements for shot 76654, the final shot in the series. Here the total emission is higher, but this is also the shot with the highest line average and central ion density. The wall model required to produce this fit had no molecular desorption from segments 14–21 and sputtering of D from segments 14–34, but used Li reflection coefficients for segments 14–34, two more segments than the previous case.

A further quantity can be derived from these results called the 'magic number' $I$ [8]. It is the ratio of calculated ionizations in the plasma core to the average H-α emissions. This ratio is expected to be constant since the cross sections for atomic hydrogen ionization vary with the electron temperature and density similarly to the cross section for excitation to the $n = 3$ level for values of $T_e$ greater than 10–15 eV. In these TFTR discharges the plasma in contact with the bumper limiter was always
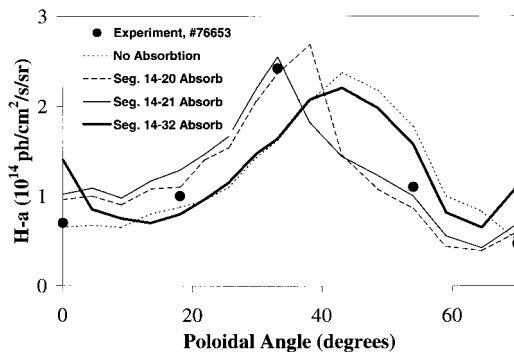
well above that threshold. The values of $I$ for the five discharges studied using the wall models described above were 7.44, 7.58, 7.42, 7.56 and $7.34 \times 10^7$ cm$^2$ sr/photon. These values are remarkably constant and very close to other simulated TFTR supershots with NBI [3]. Table 1 shows $I$ for all cases shown in this paper.

To test the individual effects of the components in the wall model several other simulations are compared to the experimental values. Fig. 5 shows the effect of varying which segments absorb. Four cases are shown for shot 76653: no absorption, absorption in seven segments (14–20), absorption in eight segments (14–21), and absorption everywhere. If there is no absorption, meaning desorption is allowed from all the segments, the peak in the distribution occurs at too high of a poloidal angle and too little H-α is produced in the middle chord. Interestingly, allowing all the carbon to absorb gives a similar profile except that the emission along the centerline and at the highest poloidal location is quite large. There is also a significant difference in $I$. No absorption anywhere gives $I = 5.85 \times 10^7$ cm$^2$ sr/photon while absorption on all segments gives $I = 7.75 \times 10^7$ cm$^2$ sr/photon.

Table 1
Ratio of ionizations inside the last closed flux surface to the total H-α emission, in units of $10^7$ cm$^2$sr/photon

| Shot # | Best fit model | Alternative conditions | | | |
|---|---|---|---|---|---|
| | | All absorbing With sputtering | All absorbing No sputtering | 8 Seg. absorbing With sputtering | 8 Seg. Sputtering No sputtering |
| 76649 | 7.44 | 5.80 | 6.11 | 7.54 | 9.32 |
| 76650 | 7.58 | | | | |
| 76651 | 7.42 | $R = 1$ 6.59 | $R =$ carbon (0.3) 7.09 | $R =$ lithium (0.15) 7.37 | $R = 0$ 7.53 |
| 76653 | 7.56 | No absorption 5.85 | 7 Seg. absorption 7.25 | 8 Seg. absorption 7.56 | All absorption 7.75 |
| 76654 | 7.34 | | | | |

Truer fits are obtained by only allowing absorption to occur at the segments which receive the most flux. There is a considerable difference however between turning on this feature from segments 14–20 vs. segments 14–21. The peak of the distribution is shifted by almost 5 degrees. The magic number for these two cases is 7.25 and 7.56 × 10$^7$ cm$^2$ sr/photon, respectively.

Physically there is a strong case for non-emission of molecules for segments 14–21. These are the segments which receive the highest ion flux and are therefore the segments which are 'conditioned' and have some of the saturated D removed from the top layer. Therefore a fast moving incident D atom or ion which does not reflect can still find a place in the C lattice and does not cause an equilibrium desorption of a molecule from the surface. As the shot sequence went on more D is placed in this high flux area but a layer of Li is also deposited there. The Li also acts as a getter allowing even more room for D atoms to be trapped without saturating the surface layer.

Fig. 6 shows the effects of turning on and off the re-emission of energetic D from sputtering for two different cases of absorption, all for shot 76649. The solid lines represent turning sputtering on and off for the case where absorption is active for segments 14–20. Note that having no sputtering produces more light from the more central (0°–38°) chords but significantly less light from the higher angle (42°–68°) chords. The values of $I$ for these two cases are 9.32 (no sputtering) and 7.54 (with sputtering) × 10$^7$ cm$^2$ sr/photon. The situation is the opposite for the cases where absorption is turned on for all the carbon segments (14–34). Then having no sputtering produces less light for most angles and more light at the very highest polodial angles(>58°). The values of $I$ for these two cases are 6.11 (no sputtering) and 5.80 (with sputtering) × 10$^7$ cm$^2$ sr /photon. This tells us that sputtering of the D from the surface is a significant source responsible for H-α light from the region which



Fig. 7. The effects of altering the reflection coefficients for shot 76651.

receives the highest flux (38°–56°) and is a major source in all low angle (<56°) regions if no molecules are emitted from any of the carbon surfaces.

Fig. 7 shows the effect of the reflection coefficients. Four variations are shown for shot 76651: all the reflection coefficients are set to zero, Li reflection coefficients (which average around 0.15 for the dominant incident energies), D-saturated-carbon reflection coefficients (which average around 0.3 for the dominant incident energies), and all the reflection coefficients are set to 1. Only a small difference in the H-α distribution is seen for the first three cases implying that the fast reflected flux is of little consequence to the overall production of H-α light seen by the HAIFA. However, note that the ratio of ionizations in the core to the density of H-α in the edge ($I$) does change considerably (Table 1). Increasing the reflection coefficients increases the number of edge ionizations relative to those deep inside the plasma which come about from the neutral beam fueling not a recycling source. The selection of Li as the wall reflection source for the best fit model shown in Fig. 3 is based on producing a value of $I$ closest to the constant value from the other shots.

## 5. Conclusion

The wall model chosen has a significant impact on both "$I$" and being able to match the experimental HAIFA data. To properly include the effect of conditioning, absorption only occurs on the segments that have the highest ion flux. This conditioning does not remove all of the embedded D, since the sputtering of D from those areas is essential to produce a good fit to the data. Once Li is added absorption on the high-particle-flux-receiving segments remains strong since Li also can trap non-reflected D. The addition of even more Li eventually builds up enough thickness such that the
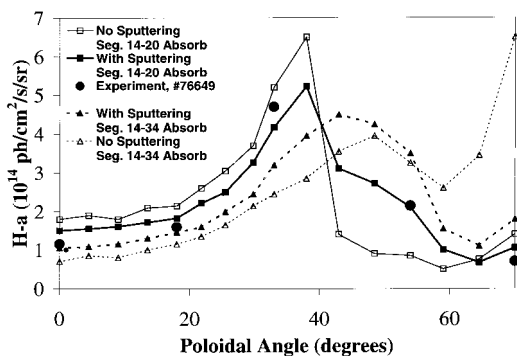


Fig. 6. The effects of allowing or disabling the sputtering of embedded D from the surface for two differing cases of absorption coefficients for shot 76649.
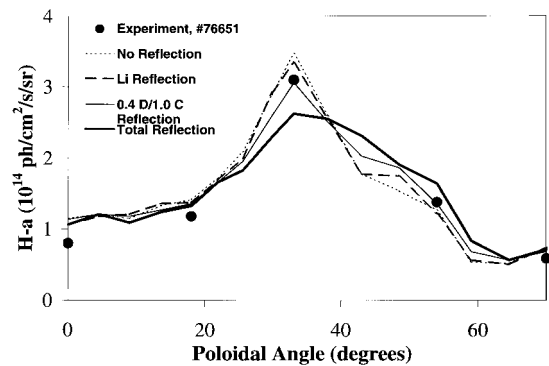
lowering of the reflection coefficient has to be included on an increasing number of segments.

## Acknowledgements

## References

[1] J.D. Strachan, et al., Phys. Rev. Lett. 72 (1994) 3526.

[2] R.V. Budny, D. Coster, D. Stotler, M.G. Bell, A.C. Jones, D.K. Owens, J. Nucl. Mater. 196–198 (1992) 462.

[3] R.V. Budny et al., Nucl. Fusion 32 (1992) 429.

[4] R.V. Budny et al., Nucl. Fusion 35 (1995) 1497.

[5] D. Heifetz, D. Post, M. Petravic, J. Weisheit, G. Bateman, J. Comput. Phys. 46 (1982) 309.

[6] D.N. Ruzic, Nucl. Instrum. Methods B 47 (1990) 118.

[7] D.P. Stotler, C.H. Skinner, R.V. Budny, A.T. Ramsey, D.N. Ruzic, R.B. Turkot, Jr., Phys. Plasmas 3 (1996) 4084.

[8] D.H. Heifetz, A.B. Ehrhardt, A.T. Ramsey, H.F. Dylla, R. Budny, D. McNeill, S. Medley, M. Ulrickson, J. Vac. Sci. Technol. A 6 (1988) 2564.

[9] A.T. Ramsey, S.L. Turner, Rev. Sci. Instrum. 58 (1987) 1211.